The Role of $\pi-\pi$ Stacking Interactions in Square Planar Palladium Complexes. Combined Quantum Mechanics/ Molecular Mechanics QM/MM Studies

Alessandra Magistrato,[†] Paul S. Pregosin,*,[†] Alberto Albinati,*,[‡] and Ursula Rothlisberger*,[†]

Laboratory of Inorganic Chemistry, ETH Zentrum, CH-8092, Zürich, Switzerland, and Chemical Pharmacy, University of Milan, I-20131 Milan, Italy

Received June 7, 2001

Density functional (DFT) studies and hybrid QM/MM-DFT calculations demonstrate the importance of $\pi-\pi$ stacking interactions in determining the structural features of two exemplary d^8 palladium complexes, $PdBr(p\text{-}NCC_6H_4)(\{S\}\text{-MeO-Biphep})$, **1**, and $PdBr(C_6F_5)$-($\{S\}$-MeO-Biphep), **2**. Despite the superficial similarity of the two compounds, the former shows marked distortions from square planar geometry, while the latter exhibits an almost ideal structure. Attractive $\pi-\pi$ stacking interactions between two pairs of P-phenyl rings and the arene backbone of the MeO-Biphep are the main origin of the distortion in complex **1**. The planar structure of complex **2** is preferred as a consequence of an additional stacking interaction between one P-phenyl ring and the pentafluorophenyl σ-ligand. The artificial introduction of an analogous stacking interaction in complex **1** reestablishes an ideal square planar geometry, thus demonstrating that switching on/off specific $\pi-\pi$ interactions distinctly alters the coordination geometry. These results reveal a previously unrecognized role for $\pi-\pi$ stacking interactions in the stabilization of structural features in transition metal compounds. This suggests $\pi-\pi$ stacking interactions as a potential new design principle in tailoring coordination compounds.

1. Introduction

The importance of $\pi-\pi$ stacking interactions between aromatic rings has been widely recognized in biological systems in (a) the stabilization of the double helical structure of DNA,[1] (b) intercalation of drugs into DNA,[1,2] (c) the tertiary structure of proteins,[3] (d) the tubular structures of cyclopeptides,[4] (e) the aggregation of porphyrin rings,[5] and (f) the conformational preferences and binding properties of polyaromatic macrocycles.[6] Attractive interactions between π-systems have been studied extensively by experimentalists and theoreticians. The simplest example of intermolecular $\pi-\pi$ interactions is provided by the benzene dimer, for which a variety of orientations such as T-shape, parallel sandwich, and parallel displaced geometries have been found that lead to stable minimum configurations.[7] Similar arrangements are observed in biological systems where the distance between planes of parallel rings in the parallel sandwich or parallel displaced geometries usually lies within 3.4−3.5 Å.[5,8]

Whereas the importance of these interactions is well established for biological systems, their role in organometallic compounds is largely unknown. Occasionally, intermolecular crystal packing $\pi-\pi$ stacking interactions stabilize specific coordination geometries.[9] However, intramolecular $\pi-\pi$ aromatic stacking interactions are rare,[10] especially within ligands of transition metal compounds[11] for which electrostatic interactions are likely to dominate over weak dispersion effects. To date, no clear evidence exists supporting aromatic attractive interactions as a decisive force for determining system-

† ETH Zentrum.
‡ University of Milan.
(1) Saenger, W. *Principles of Nucleic Acid Structures*; Springer-Verlag: New York, 1984; p 132.
(2) Wakelin, L. P. G. *Med. Res. Rev.* **1986,** *6,* 275.
(3) Burley, S. K.; Petsko, G. A. *Adv. Protein Chem.* **1988,** *39,* 125.
(4) (a) Abraham, R. J.; Eivazi, F.; Pearson, H.; Smith, K. M. *J. Chem. Soc., Chem. Commun.* **1976,** 698. (b) Abraham, R. J.; Eivazi, F.; Pearson, H.; Smith, K. M. *J. Chem. Soc., Chem. Commun.* **1976,** 699.
(5) Ranganathan, D.; Haridas, V.; Gilardi, R.; Karle, I. L. *J. Am. Chem. Soc.* **1998,** *120,* 10793.
(6) Hunter, C. A.; Sanders, J. K. M. *J. Am. Chem. Soc.* **1990,** *112,* 5525.
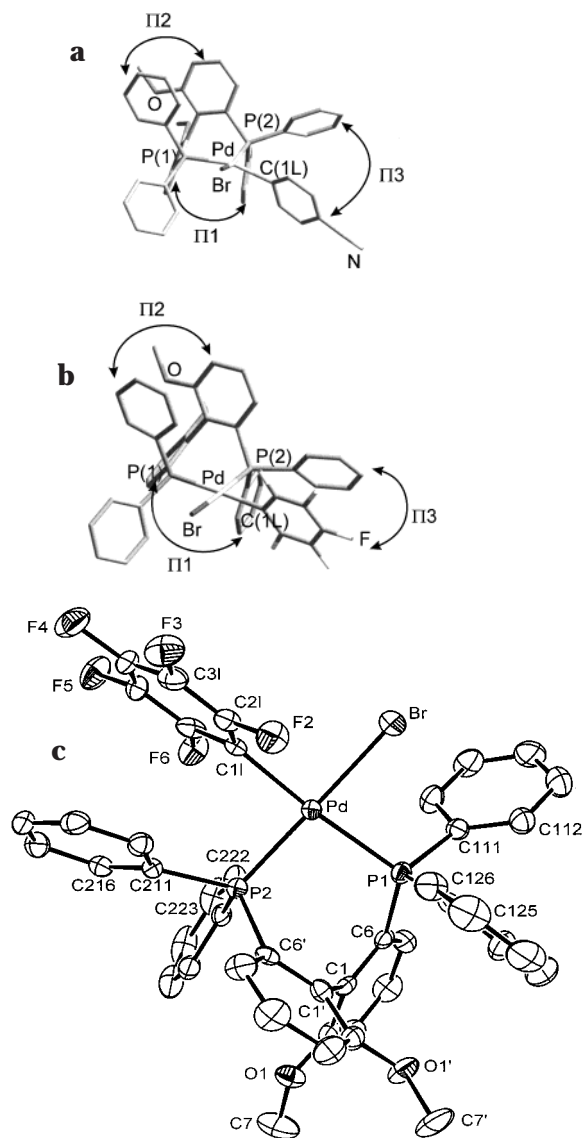
(7) Quantum mechanical calculations on the benzene dimer, e.g., (a) Chipot, C.; Jaffe, R.; Maigret, B.; Pearlman, D. A.; Kollman, P. A. *J. Am. Chem. Soc.* **1996,** *118,* 11217. (b) Hobza, P.; Selzle, H. L.; Schlag, E. W. *J. Phys. Chem.* **1996,** *100,* 18790. (c) Špirko, V.; Engkvist, O.; Soldán, P.; Selzle, H. L.; Schlag, E. W.; Hobza, P. *J. Chem. Phys.* **1999,** *111,* 572, have shown a variety of stable minimum configurations: (i) a T-shape structure with the planes of the molecules perpendicular to each other; (ii) a face-to-face geometry with the molecules on top of each other (parallel sandwich); and (iii) a parallel arrangement in which one molecule is shifted with respect to the plane of the other molecule (parallel displaced). The quadrupole−quadrupole interaction plays a significant role in stabilizing the T-shape geometry (Hobza, P.; Zahradník. *Intermolecular Complexes*; Elsevier: Amsterdam, 1988), whereas in the stacked geometries the dispersion interactions dominate. Moreover, the shifted geometry derives from a compromise between electrostatic and van der Waals interactions.
(8) Hobza, P.; Kabeláč, M.; Šponer, J.; Mejzlík, P.; Vondrášek, J. *J. Comput. Chem.* **1997,** *18,* 1136.
(9) (a) Geremia, S.; Randaccio, L.; Mestroni, G.; Milani, B. *J. Chem. Soc., Dalton. Trans.* **1992,** 2117. (b) Blake, A.; Hubberstey, P.; Li, W. S.; Quinlan, D. J.; Russel, C. E.; Sampson, C. L. *J. Chem. Soc., Dalton, Trans.* **1999,** 4261. (c) Janiak, C.; Deblon, S.; Wu, H. P.; Kolm, M. J.; Klüfers, P.; Piotrowski, H.; Mayer, P. *Eur. J. Inorg. Chem.* **1999,** 1507.
(10) Cozzi, F.; Ponzini, F.; Annunziata, R.; Cinquini, M.; Siegel, J. S. *Angew. Chem.* **1995,** *107,* 1092. (b) Lüth, M. S.; Kapinos, L. E.; Song, B.; Lippert, B.; Sigel, H. *J. Chem. Soc., Dalton Trans.* **1999,** 357.

Figure 1. Full QM models (model A): (a) PdBr(*p*-CNC$_6$H$_4$)-({S}-MeO-Biphep); (b) PdBr(C$_6$F$_5$)({S}-MeO-Biphep). Potential aromatic π−π stacking interactions are shown with arrows. (c) Crystal structure of PdBr(C$_6$F$_5$)({S}-MeO-Biphep).

atic structural distortions in relatively small organometallic compounds.

We present a systematic study performed on two prototypical chiral Pd complexes, PdBr(p-NCC$_6$H$_4$)({S}-MeO-Biphep), **1** (Figure 1a), and PdBr(C$_6$F$_5$)({S}-MeO-Biphep), **2** (Figure 1b). As shown, these complexes present three pairs of aromatic ring systems that adopt almost parallel, stacked configurations. These pairs of rings are defined as Π**1**, Π**2**, and Π**3**, where Π**1** and Π**2** refer to the aromatic rings of the P(2)- and P(1)-phenyls (for the atom numbering see Figure 1) interacting with

the rings of the biaryl backbone parallel to them, and Π**3** represents the 4-cyano/pentafluorophenyl σ-ligand and the P(2)-phenyl parallel to it. The distances between the centers of the rings are 3.6 Å (Π**1**), 3.7 Å (Π**2**), 4.3 Å (Π**3**) for **1** and 3.5 Å (Π**1**), 3.9 Å (Π**2**), 3.5 Å (Π**3**) for **2**; thus the characteristic geometrical arrangement and the separation of these pairs of rings suggest the possible presence of aromatic π−π interactions.

Density functional calculations performed on **1**[12] were not able to reproduce the observed strong distortion from square planar geometry[13] (e.g., the X-ray angles P(1)−Pd−C(1L) = 163.0° and P(2)−Pd−Br =158.9° are too small). Interestingly, the experimental structure could be fully reproduced when the aromatic ring pairs Π**1** and Π**2** of **1** were constrained to the observed experimental distances.[12] This ad hoc addition simulates the effect of attractive dispersion interactions within a DFT approach. Significant dispersion effects cannot be described in most DFT methods,[14,15] due to the local nature of the exchange−correlation approximations. However, the addition of constraints does not identify uniquely that the failure of our computational approach is due to the lack of a proper description of dispersion interactions. In addition, since constraints confine geometries to a predefined state, this retro structural approach becomes too restricted when a substantial number of rings are involved in the π−π stacking interactions. Moreover, the considerable system size prevents the use of alternative QM approaches able to account for dispersion interactions.

Here, we present mixed density functional QM/MM calculations on a series of systematically varied model systems for **1** and **2**. These hybrid models have been constructed in such a way as to selectively include or exclude attractive π−π stacking interactions, while giving the system the full freedom to relax to a favorable equilibrium geometry. In fact, no a priori constraints are applied to the system. The selective inclusion or exclusion of π−π stacking interactions was used to directly monitor the structural rearrangements induced by their presence or absence. QM/MM approaches are generally used for the study of large systems such as enzymes.[16] However, they have also been applied to catalysts,[17] where the presence of large substituents on an auxiliary play an important role with respect to activity, but a quantum mechanical treatment of the full system is too time-consuming. In QM/MM calculations

(11) (a) Castonguay, L. A.; Rappé, A. K.; Casewit, C. J. *J. Am. Chem. Soc.* **1991**, *113*, 7177. (b) Yang, F.; Fanwick, P. E.; Kubiak, C. P. *Organometallics* **1999**, *18*, 4222. (c) Selvakumar, K.; Valentini, M.; Pregosin, P. S.; Albinati, A.; Eisenträger, F. *Organometallics* **2000**, *19*, 1299. (d) Trabesinger, G.; Albinati, A.; Feiken, N.; Kunz, R. W.; Pregosin, P.; Tschoerner, M. *J. Am. Chem. Soc.* **1997**, *119*, 6315. (e) Abbenhuis, H. C. L.; Burckhardt, U.; Gramlich, V.; Köllner, C.; Pregosin, P. S.; Salzman, R.; Togni, A. *Organometallics* **1995**, *14*, 759. (f) Barbaro, P.; Pregosin, P. S.; Salzman, R.; Albinati, A.; Kunz, R. W. *Organometallics* **1995**, *14*, 5160. (g) Janiak, C. *J. Chem. Soc., Dalton Trans.* **2000**, 3885.

(12) Magistrato, A.; Merlin, M.; Albinati, A.; Pregosin, P. S.; Rothlisberger, U. *Organometallics* **2000**, *19*, 3591.
(13) Drago, D.; Pregosin, P. S.; Tschoerner, M.; Albinati, A. *J. Chem. Soc., Dalton Trans.* **1999**, 2279.
(14) Meijer E. J.; Sprik, M. *J. Chem. Phys.* **1996**, *105*, 8684.
(15) (a) Kristyan, S.; Pulay, P. *Chem. Phys. Lett.* **1994**, *229*, 175.
(16) (a) *Combined Quantum Mechanical and Molecular Mechanical Methods*; ACS Symposium Series 712; Gao, J., Thompson, M. A., Eds.; American Chemical Society: Washington, DC, 1998. (b) Rothlisberger, U.; Carloni, P.; Doclo, K.; Parrinello, M. *J. Biol. Inorg. Chem.* **2000**, *5*, 36. (c) Rothlisberger, U. *Int. J. Quantum Chem.* **1999**, *73*, 209. (d) Carloni, P.; Rothlisberger, U.; *Theoretical and Computational Chemistry*; Eriksson, L. A., Ed.; Elsevier: New York, 2001; Vol. 9, p 215. (e) Mulholland, A. J.; Lyne, P. D.; Karplus, M. *J. Am. Chem. Soc.* **2000**, *122*, 534. (f) Cui, Q.; Karplus, M. *J. Am. Chem. Soc.* **2001**, *123*, 2284. (g) Ridder, L.; Mulholland, A. J.; Rietjens, I. M. C. M.; Vervoort, J. *J. Am. Chem. Soc.* **2000**, *122*, 8728.
(17) (a) Woo, T. K.; Blöchl, P. E.; Ziegler, T. *J. Phys. Chem. A* **2000**, *104*, 121. (b) Deng, L.; Margl, P. M.; Ziegler, T. *J. Am. Chem. Soc.* **1999**, *121*, 6479. (c) Margl, P. M.; Woo, T. K.; Ziegler, T. *Organometallics* **1998**, *17*, 4997. (d) Milano, G.; Guerra, G.; Pellecchia, C.; Cavallo, L. *Organometallics* **2000**, *19*, 1343. (e) Longo, P.; Grisi, F.; Guerra, G.; Cavallo, L. *Macromolecules* **2000**, *33*, 4647.

Table 1. Bond Lengths (Å) and Angles (deg) for PdBr(*p*-CNC₆H₄)({S}-MeO-Biphep), 1, and PdBr(C₆F₅)({S}-MeO-Biphep), 2

1	X-ray	model A	model B	model C
Pd−P(1)	2.3501(9)	2.39	2.36	2.34
Pd−P(2)	2.2700(9)	2.28	2.28	2.26
Pd−Br	2.4920(4)	2.51	2.50	2.50
Pd−C(1L)	2.104(3)	2.05	2.07	2.05
P(1)−Pd−C(1L)	163.0(1)	169.1	162.1	169.6
P(2)−Pd−Br	158.96(3)	166.2	157.5	167.4

2	X-ray	model A	model C
Pd−P(1)	2.341(1)	2.36	2.30
Pd−P(2)	2.267(1)	2.29	2.26
Pd−Br	2.4656(5)	2.51	2.49
Pd−C(1L)	2.068(4)	2.05	2.05
P(1)−Pd−C(1L)	175.4(1)	171.8	178.1
P(2)−Pd−Br	174.46(3)	175.0	176.5

part of the system, such as the active region of a catalyst or of a protein, is treated by, for example, density functional calculations, while the rest of the molecule is determined using a much less expensive force field description. Assuming that a partitioning of the system between the quantum mechanical and the molecular mechanical region is chosen in an appropriate manner, it is possible to include dispersion interactions without losing the benefits of describing prominent electronic effects at the level of a first-principles method. In a QM/MM approach dispersion interactions are easily described within a classical description via, for example, a Lennard-Jones 12−6 potential. In this way, dispersion interactions between atoms in the MM part and between QM and MM atoms can be taken into account at the level of an empirical force field description.

2. Results and Discussion

For purposes of comparison, we present the X-ray structure of complex **2** and then proceed with the theoretical analysis of its structural features in relation to **1**.

2.1 X-ray Structure of PdBr(C₆F₅)({S}-MeO-Biphep), 2. Given the unusual distortion in **1**, we have determined the structure of its C₆F₅ analogue, PdBr-(C₆F₅)({S}-MeO-Biphep), **2**. An ORTEP view of **2** is shown in Figure 1c. Despite the fact that both **1** and **2** have similar donor-sets, the structure for **2** is close to an ideal square planar geometry. The immediate coordination sphere consists of the two P-donors together with the pentafluorophenyl and bromide ligands. In contrast to the previously reported structure for **1**[13] the ipso carbon of the C₆F₅ ligand and the Br atom do not deviate strongly from the P−Pd−P plane (ca. +0.04 and −0.23 Å, respectively in **2** vs +0.88 and −0.57 Å in **1**). The two Pd−P separations, 2.340(1) and 2.267(1) Å, for P(1) and P(2), respectively, are close to those found for **1** (see Table 1), whereas the Pd−C(1L) and Pd−Br separations, 2.068(4) and 2.466(1) Å, are slightly shorter. Of immediate interest are the two trans angles P(1)−Pd−C(1L) and P(2)−Pd−Br, which are both close to 175°, only slightly distorted from the ideal value of 180°. In **1** these angles were ca. 163° and 159°, respectively. Clearly, the factors determining the distinctly different structural features of these superficially similar molecules are not obvious.
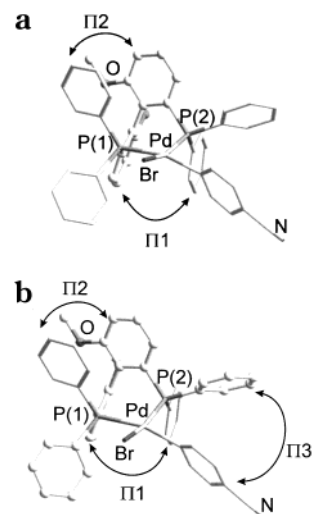

Figure 2. Hybrid QM/MM model systems for the PdBr-(*p*-CNC₆H₄)({S}-MeO-Biphep) complex. QM/MM partitioning shown for (a) model B and (b) model C. The atoms included in the quantum mechanical region are reported with lines, while the atoms included in the molecular mechanics part are represented in balls and sticks. The addition of two and three $\pi-\pi$ interactions in models B and C, respectively, is indicated with arrows.

2.2 Calculations. 2.2.1 QM/MM Models. Here we use the hybrid QM/MM approach in order to simulate the effect of $\pi-\pi$ aromatic attractive interactions within DFT-based electronic structure calculations and to systematically monitor the direct structural modifications induced by the inclusion or the exclusion of such effects.

Three different models of the system have been used in order to illustrate the structural modifications induced by the presence or the absence of specific $\pi-\pi$ stacking interactions. Model A treats the full molecule at the first-principles level. In this model we totally neglect attractive $\pi-\pi$ stacking interactions due to dispersion. In model B, the two arene moieties of the backbone are included in the molecular mechanics part and the rest of the molecule is described performing DFT calculations. Through this choice of partitioning, dispersion interactions are taken into account between the biaryl backbone and the two P-phenyl rings parallel to it (Π**1** and Π**2**, Figure 2a defines this model visually). Finally, in model C, the rings of the biaryl backbone and two rings of the P-phenyl ligands are described by a force field approach. This allows the inclusion of a third possible $\pi-\pi$ stacking interaction (Π**3** in addition to Π**1** and Π**2**) between the 4-cyano/pentafluorophenyl σ-ligand and the adjacent P-phenyl ring (Figure 2b).

2.2.2. Calculations on PdBr(*p*-NCC₆H₄)({S}-MeO-Biphep), 1. The full DFT calculations (model A) performed previously on **1**[12] resulted in significant deviations with respect to the X-ray structure. For the sake of completion, Figure 3a shows a superposition of the crystal and calculated structures for **1** using model A, and Table 1 gives bonds lengths and bond angles for the immediate coordination sphere.[12] A P(1)-phenyl group and the aryl ligand in pseudo-trans position to it represent the main areas of large deviations. The lack of agreement with respect to Π**2**[18] strongly suggests the presence of attractive $\pi-\pi$ interactions which are not
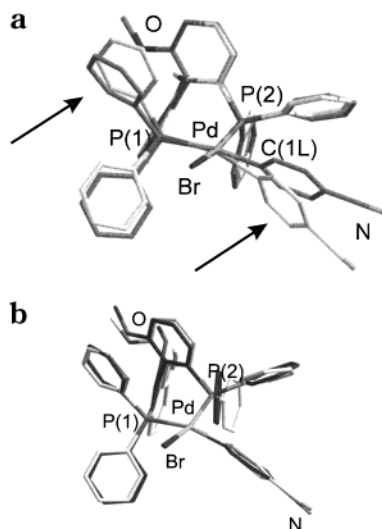
Figure 3. Superposition of the experimental structures of PdBr(*p*-CNC$_6$H$_4$)({S}-MeO-Biphep) (a) with the structure optimized at the first-principles level (model A); (b) with the structure optimized within model B. The lighter lines represent the X-ray structure, the darker lines the calculated one.

taken into account within the DFT approach.[14,15] The separations of Π**1** and Π**2** are ca. 3.6 and 3.7 Å in the X-ray structure and change to ca. 3.7 and 4.4 Å in the calculated analogue. The DFT calculations are clearly incapable of fully reproducing all of the structural features of this molecule.

A superposition of the X-ray data and the calculated structure according to the QM/MM model B (in which dispersion effects are taken into account between Π**1** and Π**2**) is reported in Figure 3b. The bond lengths and the angles of the immediate coordination sphere are also given in Table 1. All of the observed bond lengths are now reproduced within 0.03 Å (1% relative error), and the two trans angles that describe the deviation from the square planar geometry are in agreement within one degree. Clearly, the force field description of the biaryl backbone accounts for attractive π−π stacking interactions. Close inspection of Figure 2b shows that, with the force field parameters chosen here[19] for one ring of the backbone and the P(2)-phenyl parallel to it (Π**1**), the π−π stacking interactions are slightly too strong. The X-ray distances for the separations of Π**1** and Π**2** are 3.6 and 3.7 Å, respectively, whereas those for model B are ca. 3.0 and 3.4 Å, respectively. Obviously, the parameters chosen to describe the van der Waals effects slightly overestimate the actual dispersion interactions. The accuracy of these π−π stacking interactions is clearly dependent on the accuracy of the adopted force field.[8] However, our aim is to show qualitatively how the dispersion interactions can tune the structure of this complex. Consequently, we did not make any attempt to reparametrize the chosen force field.

2.2.3. Calculations on PdBr(C$_6$F$_5$)({S}-MeO-Biphep), 2. A change in the aryl ligand from the 4-cy-

---

Figure 4. Superposition of the crystal structure of PdBr-(C$_6$F$_5$)({S}-MeO-Biphep) (a) with the structure optimized at the first-principles level (model A); (b) with the structure optimized within model C. The lighter lines represent the X-ray structure, the darker lines the calculated one.

anophenyl in **1** to the pentafluorophenyl in **2** restores essentially square planar geometry. Density functional calculations on the entire structure (model A) afforded the bond lengths and bond angles reported in Table 1. The accuracy of our approach is again confirmed by the relatively small differences (at most 0.04 Å, i.e., 2% relative error) between our computational data and the observed bond lengths. However, a difference of 3.6° is observed for the P(1)−Pd−C(1L) trans angle. A superposition of the crystal structure and model A is reported in Figure 4a. The comparison of the two structures shows again that the distances between the MeO-Biphep rings and the P-phenyl rings are not correctly reproduced. Indeed, the separations between the centers of the two rings for pairs Π**1** and Π**2**, respectively, are 3.5 and 3.9 Å in the crystal data, relative to 3.7 and 4.4 Å in the calculated structure. Moreover, the separation of Π**3** involving the C$_6$F$_5$ ligand is also too large: 3.5 Å in the X-ray vs 3.9 Å calculated. Again an additional π−π stacking interaction for pair Π**3** is not adequately described. However, the local geometry is now calculated to be square planar and there is good agreement between the calculated and observed bond lengths and bond angles of the immediate coordination sphere.

The QM/MM partitioning in model C provides for the addition of three π−π stacking interactions (between Π**1**, Π**2**, and Π**3**) in **2**, and the results of these calculations are also given in Table 1. The superposition of the X-ray structure and the calculated geometry is shown in Figure 4b. The distances for pairs Π**2** and Π**3**, 3.9 Å, 3.5 Å (X-ray) and 3.8 Å, 3.6 Å (calculated), are now in good agreement. Obviously, the addition of these three π−π attractive aromatic interactions adequately reproduces the structure of the molecule, although deviations are still visible for the two rings of Π**1** (3.8 Å, X-ray, vs 3.1 Å, calculated).

Summing our results, complex **2** differs from complex **1** in that the presence of an additional π−π stacking interaction between the σ-pentafluorophenyl ligand and one of the P(2)-phenyl rings "restabilizes" the square planar arrangement. These results demonstrate a previously unrecognized large contribution of intramolecu-

---

(18) In addition, we have already pointed out[12] that there is also a significant structural rearrangement of the aryl ligand due to strong electronic correlations with the P(1)-phenyl ring in pseudo-trans position. The two rings in fact try to maximize their coplanarity within the steric restrictions of the environment.[12]

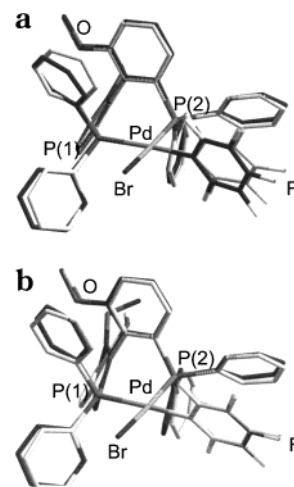(19) Clark, M.; Cramer, R. D., III; van Opdenbosh N. *J. Comput. Chem.* **1989**, *10*, 982.

lar attractive $\pi-\pi$ aromatic interactions in determining the geometry of transition metal complexes containing several aromatic moieties.

2.2.4. Effect of a Third $\pi-\pi$ Stacking Interaction in PdBr(p-NCC$_6$H$_4$)({S}-MeO-Biphep). Given the importance of this third $\pi-\pi$ interaction in **2**, we considered the effect of computationally *adding* a third $\pi-\pi$ stacking interaction between the 4-cyanophenyl and the P(2)-phenyl ring in **1**. The results of the calculation for complex **1** within model C are reported in Figure 5 and in Table 1. The calculated trans angles P(1)−Pd−C(1L) (169.6°) and P(2)−Pd−Br (167.4°) are now larger with respect to model B, and the structure approaches a square planar geometry. However, the distances for Π**1**, Π**2** (ca. 3.2, 3.3 Å) are very similar to the ones observed for model B (3.0, 3.4 Å), while the distance for Π**3** is quite short (3.4 Å in model C vs 4.6 Å in model B). This clearly indicates that, if allowed, the introduction of an additional $\pi-\pi$ stacking interaction would drive the geometry from a significantly distorted configuration to an almost square planar arrangement.

2.2.5. Analysis of the Charge Distribution. To further account for the differences in the electronic structures of the 4-cyanophenyl analogue with respect to the pentafluorophenyl derivative, not represented in our QM/MM treatment of the system, we performed a series of ring charge distribution[20] analyses. For convenience, we define the Pd-aryl ring as **R1**, the P(2)-phenyl ligand parallel to it as **R2**, and the P(1)-phenyl ring in pseudo-trans position as **R3**. These definitions and calculated charges[20] are shown in parts a and b of Figure 6 for **1** and **2**, respectively. Individual charges[20] for the three rings (calculated for complex **1** on the structure optimized within models B and C and for complex **2** on the structure optimized within model C) are reported in Table 2. Within model C, it is clear that the pentafluorophenyl ligand has a larger negative charge (ca. −0.64 e) than the 4-cyanophenyl analogue (ca. −0.49 e). The charge accumulation on the 4-cyanophenyl ligand is slightly lower (ca. −0.47 e) for the distorted geometry (model B of complex **1**). The calculated charge distribution for the P(2)-phenyl ring proximate to the 4-cyano/pentafluorophenyl ligand **R2** remains essentially constant for the three models. The observed increasing trend for the charge distribution of **R1** together with an almost constant value for the charge for **R2** suggests that the stronger electron-withdrawing properties of the C$_6$F$_5$ ligand (with respect to the p-NCC$_6$H$_4$), in addition to stronger dispersion effects, contribute to the additional $\pi-\pi$ stacking interaction between the pentafluorophenyl ligand and the parallel P(2)-phenyl. This is also shown by the charge distribution of the P(1)-phenyl ligand in pseudo-trans position to **R1**. The negative charge on this ring, ca. −0.23 e for PdBr(C$_6$F$_5$)({S}-MeO-Biphep), increases to ca. −0.32 e for PdBr(p-CNC$_6$H$_4$)({S}-MeO-Biphep) calculated within model B. These results support the previously noted strong electronic correlation connecting these rings (Figure 6a) in pseudo-trans position.[12,18]

2.2.6. Relative Strength of the $\pi-\pi$ Interactions. The relative strengths of the three $\pi-\pi$ stacking inter-

(20) The Mulliken charge analysis has been performed with a double-ζ basis without polarization function for all atoms.
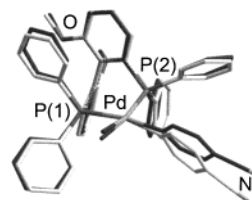

Figure 5. Superposition of the crystal structure of PdBr-(C$_6$F$_5$)({S}-MeO-Biphep) with the structure optimized within model C. The lighter lines represent the X-ray structure, the darker lines the calculated one.
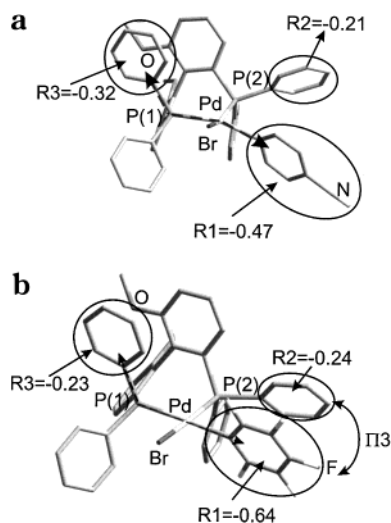

Figure 6. Charge distribution and nomenclature of aromatic rings (a) in **1** and (b) in **2**. In (b) the large electron density of the C$_6$F$_5$ ligand, in addition to larger dispersion effects, enforces trans delocalization (indicated with a dashed arrow) and induces an attractive $\pi-\pi$ interaction in Π**3** that drives the geometry back to square planar.

Table 2. Analysis of the Charge Distribution[20] for the 4-Cyano/Pentafluorobenzyl Ligand R1, the P(2)-Phenyl R2, and the P(1)-Phenyl R3 Rings Respectively Parallel and in Pseudo-Trans Position to It (Charges Are Given in Elementary Units)

	complex **1** model B	complex **1** model C	complex **2** model C
R1	−0.47	−0.49	−0.64
R2	−0.21	−0.23	−0.24
R3	−0.32	−0.30	−0.23

Table 3. Van der Waals Energies (kcal/mol) of Π1, Π2 Calculated on Model B of 1, and Π3 Calculated for Model C of 1 and 2

	Π1 (1)	Π2 (1)	Π3 (1)	Π3 (2)
van der Waals energies	−4.4	−5.1	−2.2	−3.3

actions can be qualitatively examined considering the van der Waals energies of the different pairs. The calculated van der Waals energies (Table 3) for Π**1** and Π**2** at the relative distances observed in the optimized geometry of model B are -4.4 and −5.1 kcal/mol, respectively. These values are in good agreement with the overall electronic distortion of −8.9 kcal/mol[12] in **1**. The corresponding energies for Π**3** calculated for the optimized geometry of model C of **1** and **2** are −2.2 and −3.3 kcal/mol, respectively. These energies are very sensitive to small changes in the relative distances of the two phenyl rings.[8,14] Further, van der Waals ener-

gies of −23.7 kcal/mol for PdBr(C_6F_5)({S}-MeO-Biphep), **2**, and −22.8 kcal/mol for PdBr(p-CNC$_6$H$_4$)({S}-MeO-Biphep), **1**, are found (QM/MM model C); that is, these interactions contribute significantly to the stabilization of these molecules.

3. Conclusions

We have demonstrated that π–π stacking interactions are important in determining the structural features of polyarene transition metal compounds such as the two d^8 Pd complexes **1** and **2**.

The observation of either a strongly distorted or routine square planar geometry is the result of a delicate equilibrium between the presence of an additional π–π stacking interaction between the 4-cyano/pentafluorophenyl ligand and one of the P(2)-phenyls parallel to it (Figure 6a,b) and additional electronic effects (trans delocalization between the P(1)-phenyl ring and the 4-cyano/pentafluorophenyl ligand).

In **2** the larger electron-withdrawing properties, in addition to the stronger dispersion effects of the pentafluorophenyl ligand, introduce an additional, third, π–π stacking interaction, which restores the routine geometry. The "addition" of this third attractive interaction for **1**, i.e., by switching on and off specific π–π interactions, is sufficient to turn the observed distorted geometry into an ideal square planar arrangement.

We believe this to be the first application of the QM/MM approach to assess the importance of weak interactions in basic coordination geometry. Given that bidentate polyarene ligands find increasing use in homogeneous catalysis, it will be necessary to consider π-stacking interactions in discussing the properties of their complexes.

4. Experimental Section

4.1. Computational Details. All the DFT calculations were performed using the Amsterdam Density Functional (ADF2000.01) program.[21] The electronic configurations of the molecular systems were described by a triple-STO basis set on the transition metal center for the ns, np, nd, $(n+1)$s, and $(n+1)$p valence shells, whereas a double-STO basis set was used for Br (4s,4p), F (2s,2p), C (2s 2p), N (2s,2p), O (2s,2p), and H (1s). The inner shells of the atoms were treated within the frozen core approximation. Gradient-corrected calculations with the exchange functional of Becke[22] and the correlation functional of Perdew[23] have been used. First-order scalar relativistic corrections[24] were included for the palladium atom. A spin-restricted formalism was used throughout all the calculations.

The Tripos 5.2 force field[19] was used for the molecular mechanics potential, augmented for Pd according to the universal force field of Rappé et al.[25] The dispersion coefficients of the Tripos[19] force field for the atoms involved in π–π stacking interactions considered here are reported in Table 4.

(21) (a) Baerends, E. J.; Ellis, D. E.; Ros, P. *Chem. Phys.* **1973**, *2*, 41. (b) Versluis, L.; Ziegler, T. *J. Chem. Phys.* **1998**, *88*, 322. (c) te Velde, G.; Baerends, E. J.; *J. Comput. Phys.* **1992**, *99*, 84. (d) Fonseca Guerra, C.; Snijders, J. G.; te Velde, G.; Baerends, E. J. *Theor. Chim. Acc.* **1998**, *99*, 391.
(22) Becke, A. *Phys. Rev. A* **1988**, *38*, 3098.
(23) Perdew, J. P.; Zunger, A. *Phys. Chem. Rev. B* **1981**, *23*, 5048.
(24) (a) Snijeders, J. G.; Baerends, E. J. *J. Mol. Phys.* **1978**, *36*, 1789. (b) Snijders, J. G.; Baerends, E. J.; Ros, P. *Mol. Phys.* **1979**, *38*, 1909.
(25) Rappé, A. K. Casewit, C. J.; Colwell, K. S.; Goddard, W. A., III; Skiff, W. M. *J. Am. Chem. Soc.* **1992**, *114*, 10024.

Table 4. Empirical Parameters of the Tripos Force Field[19] for the Lennard-Jones 12−6 Potential $V(r) = 4\epsilon[(\sigma/r)^{12} - (\sigma/r)^6]^a$

	ϵ	σ
H	0.042	3.00
C	0.107	3.40
O	0.116	3.04
N	0.095	3.10
F	0.109	2.94

^{a} σ (Å) represents the van der Waals bond length and ϵ (kcal/mol) the well depth.

Table 5. Experimental Data for the X-ray Diffraction Study of PdBr(MeO-Biphep)(C_6F_5), 2

formula	$C_{44}H_{32}BrF_5O_2P_2Pd$
mol wt	935.95
data coll T, K	200(2)
diffractometer	Bruker SMART CCD
cryst syst	monoclinic
space group (no.)	$P2_1$ (4)
a, Å	10.7794(1)
b, Å	13.9492(2)
c, Å	13.6053(1)
β, deg	91.62(4)
V, Å^3	1975.89(4)
Z	2
$\rho_{(calcd)}$, g cm^{-3}	1.573
μ, cm^{-1}	16.22
radiation	Mo Kα (graphite monochromated $\lambda = 0.71073$ Å)
θ range, deg	$1.55 < \theta < 25.59$
no. of ind data	6575
no. obs. reflns (n_o) $[|F_o|^2 > 2.0\sigma(|F^2|)]$	5890
transmn coeff	0.81−0.94
no. of params refined (n_v)	496
R (obsd reflns)^a	0.031
R_w^2 (obsd reflns)^b	0.063
GOF	0.860

^{a} $R = \sum(|F_o - (1/k)F_c|)/\sum|F_o|$. ^{b} $R_w^2 = \{[\sum w(F_o^2 - (1/k)F_c^2)^2/\sum w|F_o^2|^2]\}^{1/2}$.

We have chosen a purely sterical coupling;[26] that is, only bonded and van der Waals interactions between the QM and the MM part are included with no coupling of the electrostatic interactions. Thus, dispersion interactions between the QM and MM part are considered by the addition of empirical dispersion coefficients on both the MM and QM atoms describing the van der Waals interactions on a purely empirical basis.

In QM/MM models B and C the arenes and the phenyls included in the MM part are simply replaced by hydrogen atoms in the electronic structure calculations in order to saturate the valence of the boundary P atoms. As a consequence, the electronic properties of these substituents are simply replaced by the electronic properties of hydrogen atoms.

4.2. Crystallography. Structural Study of PdBr(MeOBiphep)(C_6F_5), 2. Yellow crystals of PdBr(MeOBiphep)-(C_6F_5) **2** suitable for X-ray diffraction were obtained by crystallization from pentane/ether/methylene chloride and are air stable. A prismatic single crystal was mounted, for the data collection, on a glass fiber at a random orientation, on a Bruker SMART CCD diffractometer at 200 K. The space group was determined from the systematic absences, while the cell constants were refined, at the end of the data collection, with the data reduction software SAINT.[27] Data were collected by using scans in steps of 0.3 deg; a list of experimental conditions for the data collection is given in Supplementary Table S1. The collected intensities were corrected for Lorentz and

(26) Woo, T. K.; Cavallo, L.; Ziegler, T. *Theor. Chem. Acc.* **1998**, *100*, 307.
(27) *SAINT*, SAX Area Detector Integration; Siemens Analytical Instrumentation, 1996.

polarization factors[27] and empirically for absorption using the SADABS program.[28]

Selected crystallographic and other relevant data are listed in Table 5 and in Supplementary Table S1. The standard deviations on intensities were calculated in term of statistics alone, while those on F_o^2 were calculated as shown in Table S1. The structure was solved by direct and Fourier methods and refined by full matrix least squares,[29] minimizing the function $[(w(F_o^2 - (1/k)F_c^2)^2]$. Anisotropic displacement parameters were used for all atoms except the hydrogens. Their contribution, in calculated positions (C—H = 0.95 (Å), B(H) = 1.5B (Cbonded) (Å²)), was included in the refinement using a riding model. No extinction correction was deemed necessary. Upon convergence (see Supplementary Table S1) the final Fourier difference map showed no significant peaks. Refining

the Flack's parameter[30] tested the handedness of the structure. All calculations were carried out by using the PC version of the SHELX-97 programs.[29] The scattering factors used, corrected for the real and imaginary parts of the anomalous dispersion, were taken from the literature.[31]

Supporting Information Available: Tables of bond lengths and angles, complete atomic coordinates, anisotropic displacement coefficients, and isotropic displacement coefficients for hydrogen atoms, and an ORTEP plot with a full numbering scheme. This material is available free of charge via the internet at http://pubs.acs.org.

(28) Sheldrick, G. M. *SADABS*; Universität Göttingen.
(29) Sheldrick, G. M. *SHELX-97*, Structure Solution and Refinement Package; Universität Göttingen, 1997.

(30) Flack, H. D. *Acta Crystallogr.* **1983**, *A 39*, 876.
(31) *International Tables for X-ray Crystallography*; Wilson, A. J. C., Ed.; Kluwer Academic Publisher: Dordrecht, The Netherlands, 1992; Vol. C.